PNAS
www.pnas.org

Supplementary Information for

A monumental cemetery built by eastern Africa's first herders near Lake Turkana, Kenya

Elisabeth A. Hildebrand, Katherine M. Grillo, Elizabeth A. Sawchuk, Susan K. Pfeiffer, Lawrence Conyers, Steven T. Goldstein, Austin (Chad) Hill, Anneke Janzen, Carla E. Klehm, Mark Helper, Purity Kiura, Emmanuel Ndiema, Cecilia Ngugi, John J. Shea, Hong Wang

Corresponding author: Elisabeth Hildebrand
Email: Elisabeth.Hildebrand@stonybrook.edu

This PDF file includes:

www.pnas.org/cgi/doi/10.1073/pnas.1721975115

Supplementary text

Excavation methods

Excavations of the Lothagam North platform (field seasons during 2009, 2012, 2013, and 2014) included a 1x5 m trench on the platform's west side, a 2x2 unit in the central mortuary cavity, and a 1x1 test unit on the eastern edge of the platform. Two additional 1x1 test units explored surface features just east of the platform. Farther from the platform, excavations probed one stone circle (1x2 m unit), and the largest cairn (1x4 m unit). Excavations followed natural stratigraphic breaks and employed 5-cm arbitrary levels within a continuing stratum. All sediment was sieved through 2 mm mesh buttressed by 5 mm screening. Matrix was characterized in terms of particle size (1), color (2), and compaction. Inclusions were recorded by size class (1), dominant materials (e.g., basalt), frequency, and angularity. Boulders and cobbles >15 cm were plotted individually, noting materials, shape/angularity, and inclination.

Spatial data collection

In 2009, two 1x1 test units (excavated without a Total Station) revealed a high density of artifacts and the top of two burials that were immediately re-covered to await bioarchaeological specialists. Every subsequent field season employed a Total Station: Leica EDM (2012, 2013), and Nikon Nivo with CarlsonSurvPC software running on a Windows tablet (2014). Survey in 2013 utilized a Topcon GR-5 Real Time Kinematic (RTK) GPS system. In 2013 and 2014 spatial surveys using Unmanned Aerial Vehicles (UAVs) and Pole Aerial Photography (PAP) from heights of 8-80 m allowed high-resolution mapping. Aerial photographs of the site and surrounding landscape were recorded from a combination of fixed wing and rotary wing UAVs. These photographs, along with Ground Control Points established via Total Station and RTK GPS, were processed in Photoscan Pro software to produce georeferenced Digital Elevation Models (DEMs) and undistorted orthophotographs. From these data sources, accurate maps of the site, with a resolution of approximately 1 cm/pixel, were produced. DEMs also served as a baseline for Ground-penetrating Radar (GPR), described in detail below in Figure S3.

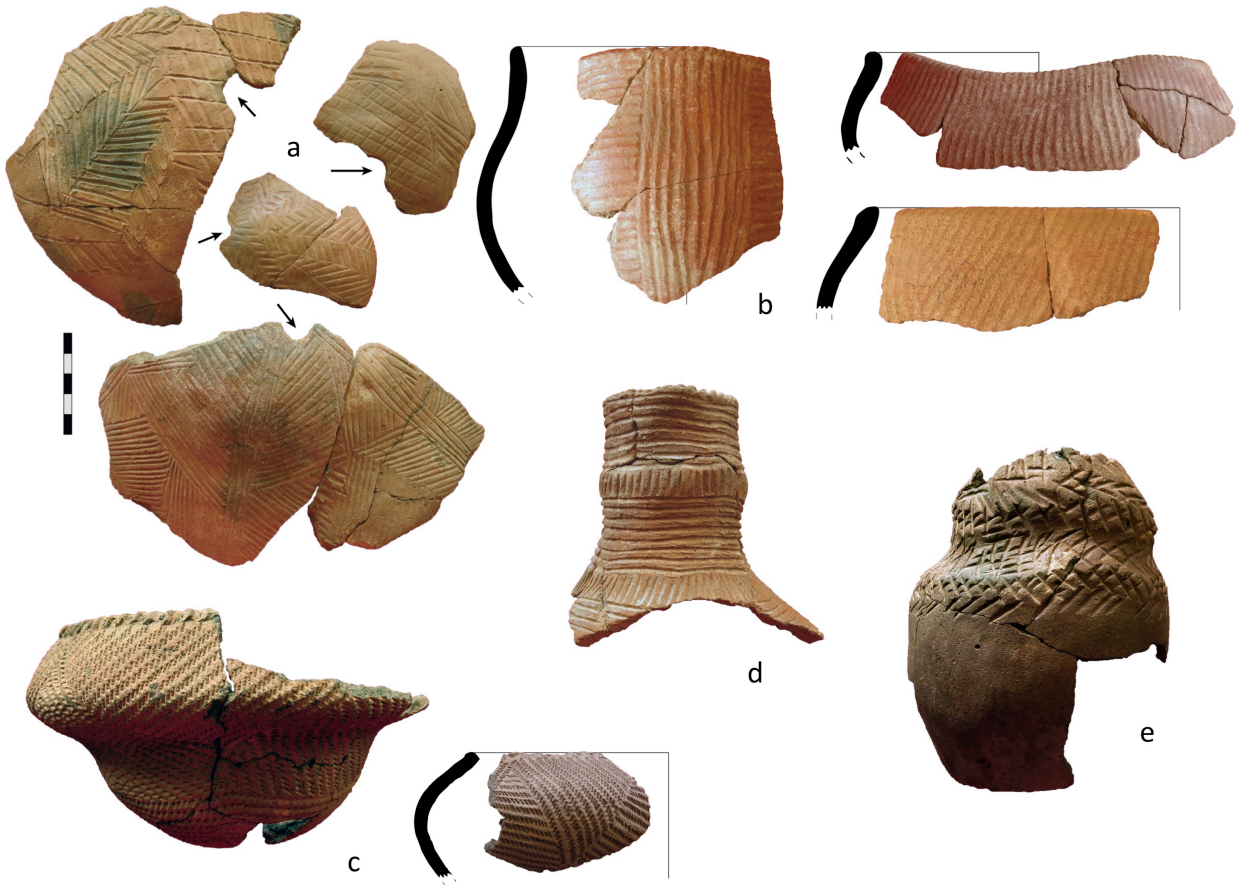

Figure S1. Sample of partial ceramic vessels found at Lothagam North Pillar Site (GeJi9). All can be considered "Nderit" as broadly defined by Nelson (1); note the reddish paint/wash on most exterior surfaces, fine well-fired sandy pastes, and the wide range of formal and decorative variation. Those in group *a* are shallow bowls with incised decorations in geometric patterns, and these vessels have had holes intentionally drilled at their bases, post-firing and possibly causing these vessels to break. Vessels in group *b* can be categorized as the "burnished ripple" variant of Nderit; most exhibit large, more globular forms. Vessels in group *c* can be considered "Classic Nderit," the earliest-defined variant of Nderit Ware. These vessels are typically open-mouthed bowls, but note the tiered shape of the vessels on the left. Classic Nderit pots typically have rouletted decoration in panels entirely covering exterior surfaces, perhaps imitating basketry, and are sometimes internally scored. Vessel *d* is a bottle with incised decoration. Vessel *e* has been termed the "learner's pot." It appears gourd-shaped, is roughly formed, and has unusually irregular or unpracticed incising on its neck and shoulder, as if made by a child.

Figure S2: Ceramic figurines from Jarigole Pillar Site (GbJj1).
a honey badger, front and side view; *b* possible bovine figure; c possible bovine figure, side and front view; *d* unidentified figure; *f* leopard; *g* bovine figure; *h* giraffe; *i* hippopotamus, front and top view; *j* and *k* elephants.

Figure S3. Excavation, spatial data collection, and Ground-penetrating Radar (GPR) detection of mortuary cavity at GeJi9.

Ground-penetrating radar (GPR) (18) were collected with a GSSI SIR-3000 control system using 400 MHz antennas and a survey wheel for distance calibration. Radar reflection data were collected in a grid with profiles spaced at 50 cm intervals, with 40 reflection traces digitized every meter along transects. The grid was 20x22 m in maximum dimension, but there are a few areas around the periphery where the abundance of large surface stones made data collection impossible. Each reflection profile was corrected for velocity and radar wave travel times were converted to depth in the ground for two-dimensional display. An example of one reflection profile (Fig. S3*a*, below) shows both corrected depth and two-way radar travel time in nanoseconds on the vertical axes. All reflections were filtered to remove frequencies <200 MHz and >800 MHz with a composite noise trace subtracted from all digital values to remove background noise. Although the irregular ground surface caused abundant energy coupling errors as the antenna was pulled over a variety of stones and pebbles, all reflections are displayed un-averaged so that every reflection in the ground is visible in two dimensions. This tends to produce a somewhat irregular pattern in profile views of reflections generated from horizontal and sub-horizontal layers.

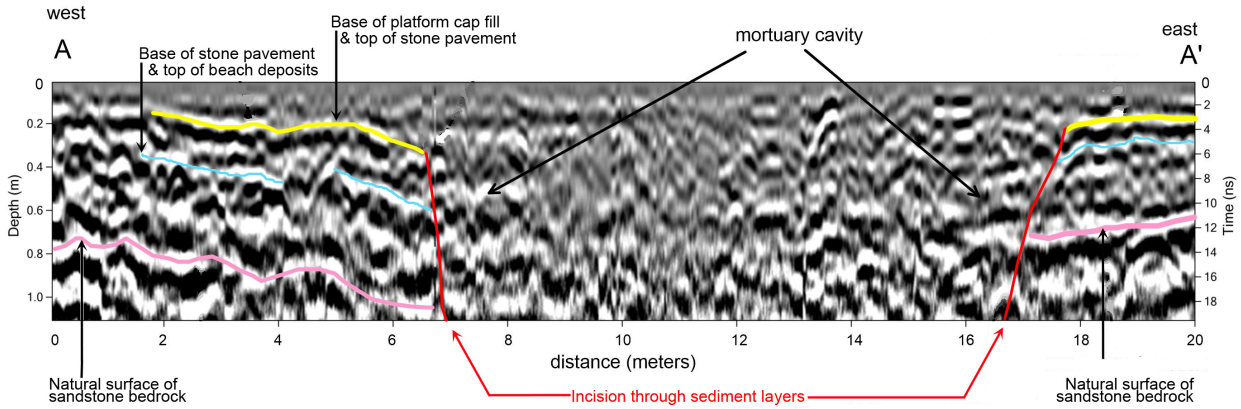

a Ground-Penetrating Radar (GPR) reflection profile running east-west across the platform of Lothagam North Pillar Site (GeJi9). The natural top of the sandstone bedrock (pink line) can be detected on the western side of the platform (0.7-1.0 m below surface) and on the eastern side of the platform (0.7-0.8 m below surface). GPR reflections in profile are consistent with observations of bedrock during excavation. Above the bedrock, bedded deposits (early Holocene beach sands, overlain by a stone pavement) produce a reflections consistent with relatively horizontal sediment strata. Stone pavement deposits (blue line=base, yellow line=top) are thicker on the west side of the platform (confirmed by observation in excavation units N04E37-39), and thinner on the east side of the platform (confirmed by observation in excavation unit N04.25E52). The incision cuts at the edges of the central mortuary cavity are visible in GPR reflection profiles as truncations of the layered sediments (red lines). Mortuary deposits within the truncated area appear in GPR profiles as a mostly heterogeneous fill unit and produce reflections with no layering and only a few point-source reflections generated from larger stones. Due to the removal of bedrock to make burial pits, the bedrock surface below the mortuary cavity is deeper than the depth of radar energy penetration, so cannot be detected via GPR. Platform cap deposits overlie both the mortuary cavity and the stone pavement. GPR reflections show no distinction between mortuary cavity fill vs. cap fill in the center of the platform. However, near the surface radar reflections demarcate the boundary between the stone pavement and the cap deposits (yellow line) along the margin of the platform.

b Plan-view image showing re-gridded amplitude values at 80-120 cm depth. Colored areas signify high-amplitude reflections from bedded layers such as the stone pavement and early Holocene beach deposits. White areas indicate that radar reflections are of a very low amplitude or absent altogether; this suggests there are no layers to reflect radar, and sediments are essentially homogenized. Human remains that are known to be abundant in these homogenized fill units within the incision boundaries are too small to reflect energy, and appear as areas of no or small amplitude reflections. A clear contrast between high-amplitude and low-amplitude reflections establishes the border of the mortuary cavity incision (red line).

The linear white area was unavailable for GPR survey due to open excavations.

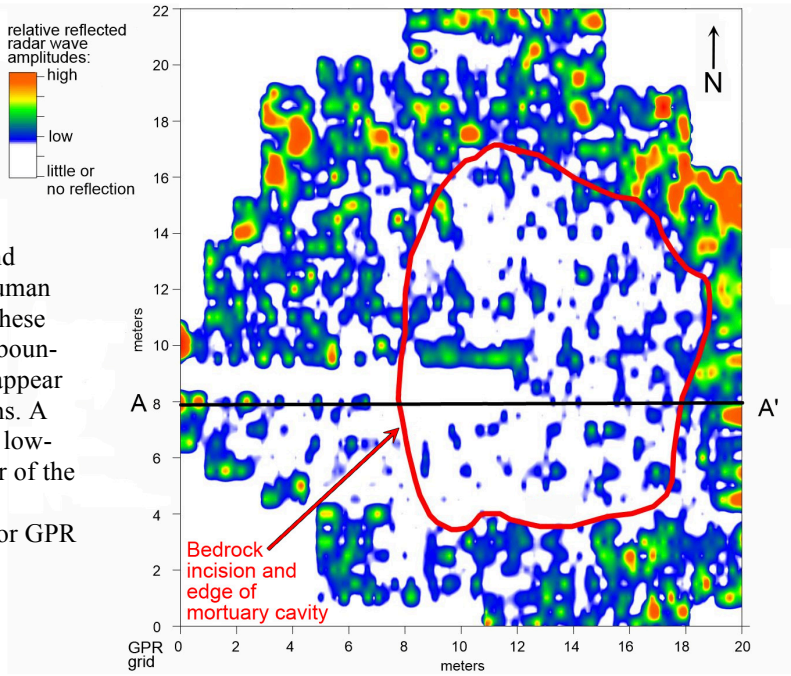

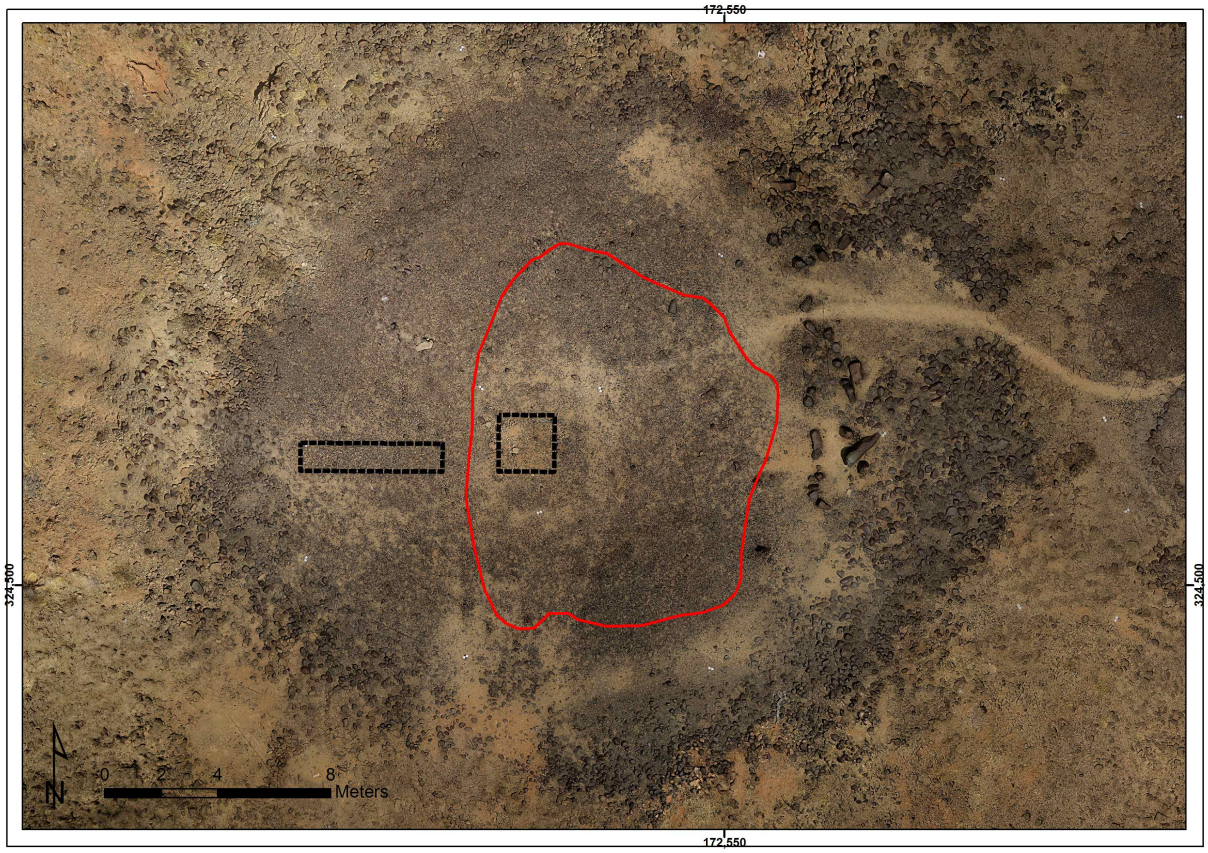

c Orthoimage of the main platform at Lothagam North. Images were recorded with a PAP setup (pole aerial photography) and processed with Agisoft Photoscan Pro. The red line indicates the location of the main cut location derived from the GPR data (outlining the edge of the mortuary cavity), while the black lines indicate the excavation extent in 2014.

Figure S4: Radiocarbon sample collection, preparation, AMS analysis, and calibration.
All charcoal fragments >2 mm and all ostrich eggshell beads or fragments were regarded as potential samples for radiocarbon dating. Ostrich eggshell is suitable for radiocarbon dating in the Lake Turkana area because no limestone outcrops exist regionally and any small amount of soil carbonates, if swallowed by ostriches, would be digested by the strong acid in their stomach. Radiocarbon dates of ostrich eggshell are more reliable than those on bone or charcoal because eggshells are impervious to post-depositional alteration (*SI Refs* 5, 6). Each charcoal chunk or ostrich eggshell fragment detected *in situ* was piece-plotted, collected and handled using metal spoons or tweezers, wrapped in aluminum foil to provide physical protection, and placed into its own plastic bag. Ostrich eggshell beads occurred both individually and in clusters, and were subject to the same anti-contamination measures described above; clustered beads were collected together, and only isolated beads were considered potential dating samples. Charcoal and ostrich eggshell found via sieving were not preferred for dating due to less precise contextual information and greater potential for contamination; however, they were handled using metal spoons or tweezers, individually wrapped in foil, and bagged. All but two dates from Lothagam North are from *in situ* plotted finds. ISGS A-2649 was recovered from sieving fill above Burial 6 in the stone circle; this feature yielded no plotted dating samples. ISGS A-2625 was recovered from sieving a limited set of sediments closely associated with the cranium of Burial 2 in the mortuary cavity, and hence has tight context. Eight samples (three charcoal, five ostrich eggshell) were submitted to the Radiocarbon Dating Laboratory at the Illinois State Geological Survey (ISGS), Prairie Research Institute, University of Illinois at Urbana-Champaign between 2009 and 2016.

Charcoal samples were given standard ISGS acid-base-acid (ABA) pretreatment: boiling for 1 h in 2M HCl and rinsing to neutrality with DI H_2O; soaking in cool 0.125 M NaOH for 1 h and rinsing to neutrality with DI H_2O; soaking in 2M HCl for 30 min and rinsing to pH 6 with DI H_2O, and drying overnight in an oven at 80°C. The same pretreatment was applied to ISGS ^{14}C-free wood background and wood working standard samples – including IAEA C5 (Two Creek forest wood), and FIRI-D (Fifth International Radiocarbon Inter-comparison D wood) (*SI Ref* 7). At ISGS, archaeological charcoal and wood background and working standards were combusted in sealed quartz tubes with minimal amount of CuO granules in preheated quartz tubes for combustion (2 h at 800°C). Tubes were then cooled from 800 °C to 600 °C for 6 h so CuO would reduce the nitrogen oxides to nitrogen gas.

Ostrich eggshell (OES) consists of mammillary (inner), palisade (outer), and cuticle layers (*SI Ref* 8). The palisade layer contains many pore canals, and has generally poorer crystallinity and higher porosity than the inner layer (*SI Ref*s 8, 9). This outer layer is likely susceptible to secondary carbonate accumulation but the inner layer is highly resistant to diagenesis and was isolated here for AMS ^{14}C dating. The exterior layer of OES was completely removed using a razor blade. The clean inner layer that contains dense crystalline structure was gently crushed into ~ 2 mm grains using a pre-acidified mortar and pestle. About 50 mg of sample was placed in the main chamber and 2 ml of 100% phosphoric acid was transferred to the arm chamber of the reaction vessel. The vessel was evacuated to <5 mTorr vacuum condition. The initial CO_2 of the acid hydrolysis during the first 20 minutes was removed by vacuum. The hydrolysis continued overnight at room temperature. This approach was also applied to the ^{14}C-free limestone blank and reference material of TIRI-I (Third International Radiocarbon Inter-Comparison sample I) travertine samples. Purified CO_2 of OES, limestone blank, and TIRI-I was collected cryogenically under <5 mTorr vacuum condition.

Purified CO_2 from all charcoal and OES samples was submitted to the Keck Carbon Cycle AMS Laboratory of the University of California-Irvine for AMS ^{14}C analysis using the hydrogen-iron reduction method with δ^{13}C values measured on prepared graphite (*SI Ref* 10). All results have been corrected for isotopic fractionation (*SI Ref* 11). The AMS analysis indicated that after blanks subtraction, the FIRI-D and IAEA-C5 working standard of wood and the TIRI-I working standard of travertine reference materials yielded target values within 2σ deviations. For all results, isotopic fractionation correction (*SI Ref* 11) used AMS spectrometer measurements of δ^{13}C values on prepared graphite.

Probability distributions (95.4%) for age ranges obtained from Lothagam North Pillar Site appear on the following page.

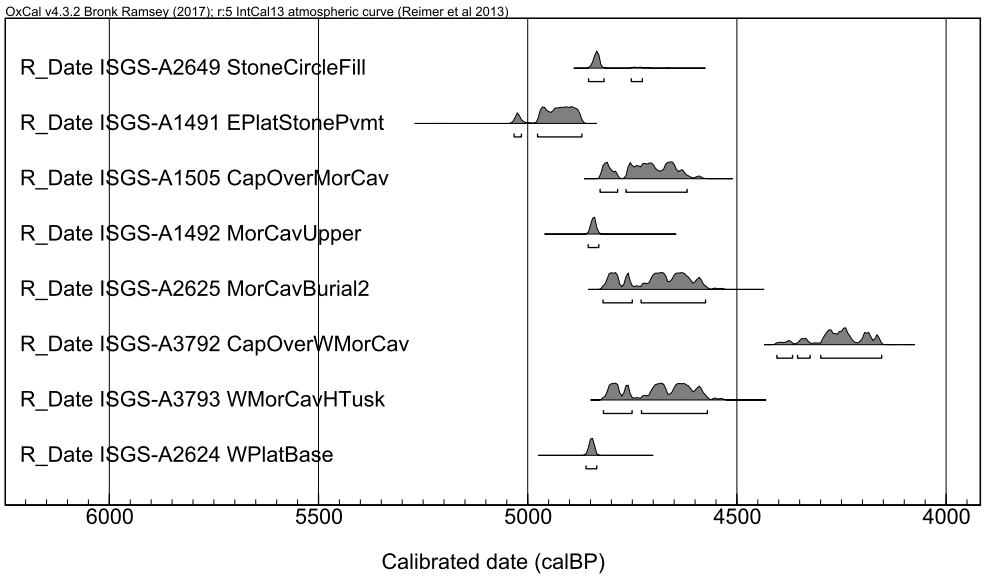

a Multiplot showing probability distributions (95.4%) of dates calibrated via OxCal v4.3.2 (*SI Ref* 11), which employs the IntCal13 calibration curve (*SI Ref* 12). Age ranges are presented in order moving east to west across the site. GeJi9's oldest date is from the stone pavement at the base of the east side of the platform. Slightly later and more tightly defined dates were obtained from a similar context on the west side of the platform, from upper parts of the mortuary cavity, and from fill in the stone circle. Later dates with larger age ranges come from deposits in and above the mortuary cavity.

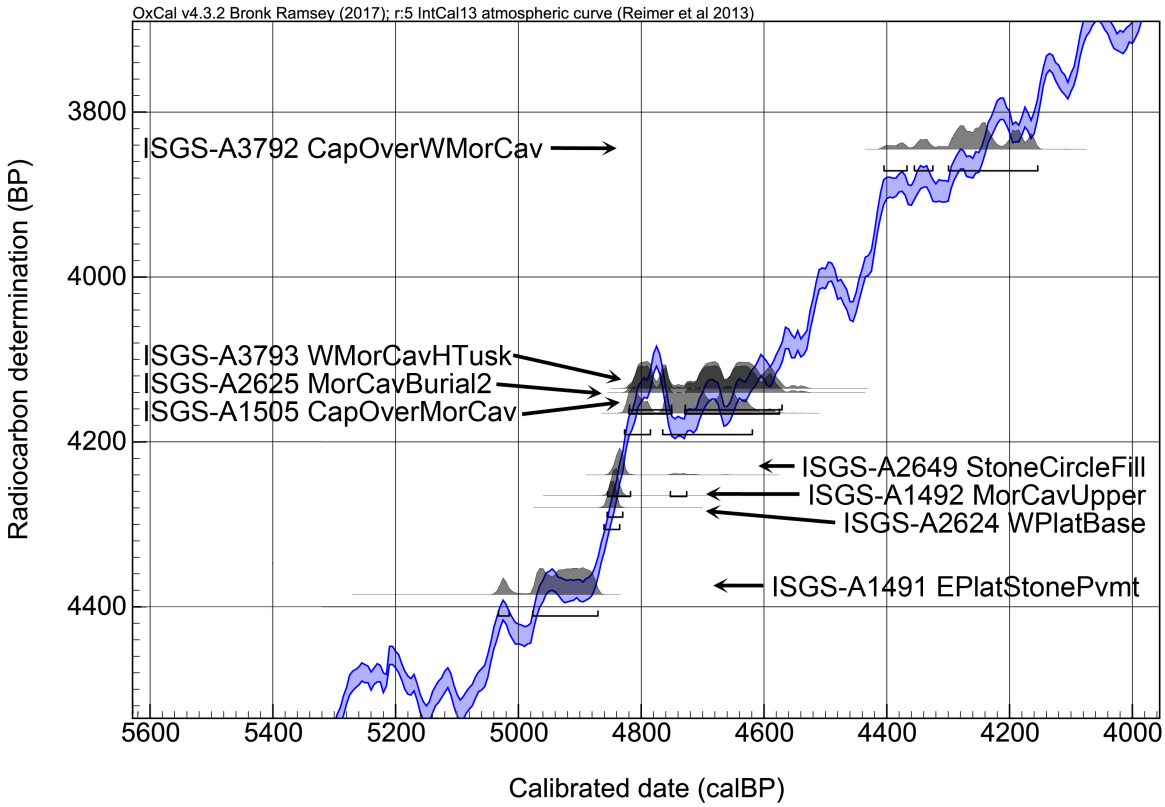

b Age range probability distributions (95.4%) plotted against the radiocarbon calibration curve, showing why dates cluster into four distinct groups. Large age ranges correspond to times of fluctuating atmospheric radiation.

Figure S5: Stone and mineral identification of pendants and earrings from the Lothagam North excavations in 2012-2014.

Bead rock and mineral identification relied mainly on characteristics visible to the unaided eye and at up to 40X magnification (e.g. color, texture, grain size, luster, cleavage, relative toughness and hardness from abrasion and wear), supplemented by measurement of specific gravity, response to a hand magnet, and reaction to long- and short-wavelength ultraviolet light. Between one and four beads of each type were chosen as 'type specimens' for specific gravity testing. Specific gravities were determined by the hydrostatic weighing technique using a balance accurate to 0.001 grams using the average of three or more replicate measurements. Photos were obtained with a digital SLR camera, and a stand-mounted high magnification video camera (Dino-lite) that allowed up to 200x magnification to examine other identifying characteristics as well as use-wear and surface marks. A select number of stone beads were loaned, with approval from the National Museums of Kenya, to the Department of Geosciences at the University of Texas at Austin in order to conduct nondestructive materials analysis through Raman spectroscopy, x-ray diffraction (XRD) and scanning electron microscopy energy dispersive analysis (SEM-EDX) that could not be done in Kenya. The advanced analytical techniques identified the mineralogy of some of the previously unconfirmed bead materials, including analcime, scolecite-mesolite, and talc with magnesiochromite. The borrowed materials were returned to Kenya in March 2016.

Pendants: 1-9, volcanics. **10**, unknown iron precipitate. **11-24**, amazonite. **25**, talc. **26-32**, analcime. **33-37**, carnelian (chalcedony). **38-40**, fluorite. **41**, limestone. **42**, chlorite schist. **43**, hematite cemented sandstone. **Earrings: 44**, limestone. **45**, scolecite. **46-49**, amazonite.

Table S1: Bioarchaeological analysis of human remains recovered from Lothagam North.
Detailed information on procedures for recovery, documentation, and analysis is given below the table.

Burial number	Number of individuals	Burial type	Estimated age at death	Estimated sex
Burials from the 2x2 m excavation unit in the mortuary cavity (central platform)				
GeJi9-B1	1	Primary articulated	Older adult	Male
GeJi9-B2	1	Primary articulated	Younger adult	Male
GeJi9-B3	1	Primary articulated	Middle adult	Male
GeJi9-B4	1	Primary articulated	Adult	
GeJi9-B5	1		Newborn	
GeJi9-B7	1	Primary articulated	Infant (0.5-1 year)	
GeJi9-B8	1	Primary articulated	Newborn	
GeJi9-B9	1	Primary articulated	Adult	Female
GeJi9-B10	1	Primary articulated	Child (7.5-10.5 years)	
GeJi9-B11	1	Primary articulated	Younger adult	Female
GeJi9-B12	1	Primary articulated	Middle aged adult	Male
GeJi9-B13	1	Secondary bundle	Adult	Male?
GeJi9-B14	1	Primary articulated	Adult	Female?
GeJi9-B15	3	Primary articulated	Middle aged adult	Female?
			Adult	Female?
			Adult	
GeJi9-B16	2	Primary articulated	Adult	
		Secondary bundle	Adult	
GeJi9-B17	1	Primary articulated	Adult	Male?
GeJi9-B18	2	Primary articulated	Younger adult	Male
			Middle aged adult	Male
GeJi9-B19	1	Primary articulated	Teenager (16.5 years)	Female?
GeJi9-B20	1	Primary articulated	Adult	Female?
GeJi9-B21	2	Primary articulated	Younger adult	Male?
			Younger adult	Female?
GeJi9-B22	2	Primary articulated	Adult	Male?
			Adult	
GeJi9-B23	1	Primary articulated	Adult	Female
GeJi9-B24	3	Primary articulated	Adult	Female
			Adult	
			Infant (4.5 months)	
GeJi9-B25	1	Primary articulated	Older adult	Male
GeJi9-B27	1	Primary articulated	Older adult	
GeJi9-B28	1	Primary articulated	Middle aged adult	Female
GeJi9-B30	1	Primary articulated	Older adult	Male
GeJi9-Burial A	1		Infant (1.5-4.5 months)	
Burials on the periphery of the mortuary cavity (western side of platform)				
GeJi9-B26	4	Primary articulated	Older adult	Male
		Secondary bundle	Adult	
			Middle aged adult	Male
			Younger adult	Male
GeJi9-B29	1	Primary articulated	Middle aged adult	Male?
Burial in the stone circle (50 m east of the platform)				
GeJi9-B6	3	Secondary bundle	Older adult	Male
			Adult	
			Juvenile	

Recovery and documentation of human remains followed standard protocols for exposure, mapping, and documentation with some modifications for high heat, high UV conditions. Skeletons were excavated under UV umbrellas and elements selectively stabilized with consolidant (Butvar B-98). Consolidant was not applied to associated artifacts (e.g., adornments) or tooth crowns, and untreated bone and tooth samples have been set aside for future analysis. Once exposed, burials were documented *in situ* using a Total Station and photographed for 3D

photogrammetry prior to removal. Beads and other adornments associated with burials were mapped and collected separately. Secondary bundle burials—disarticulated, liner arrangements of predominantly long bones representing one or more individuals—were documented and removed following an established ossuary procedure in which each bone is numbered and photographed from a single point (*SI Ref* 14). Given the dense, overlapping nature of burials in the central platform's mortuary cavity, recovery focused only on remains lying entirely within the excavation units. Skeletal elements visible in the walls were documented but not removed.

Laboratory methods at the Turkana Basin Institute included bone cleaning, further consolidation (if required), and minor reconstruction. Osteological methods followed standard procedures (*SI Refs* 15, 16). Age at death in juveniles was determined through dental development and epiphyseal fusion (*SI Refs* 17, 18). Adulthood was determined by presence of third molars, epiphyseal fusion, and overall size. Adult age at death was estimated by age-related osteological changes (e.g., at the pubic symphyses, auricular surfaces, and sternal rib-ends) in conjunction with indicators such as degree of dental wear, cranial suture obliteration, and presence of degenerative joint disease. Wherever possible, adults were grouped into younger (18-30 years), middle aged (30-50 years), and older (50+ years) categories. Adult sex was determined by pelvic and cranial morphology following standard practice. Where preservation permitted, individuals were assessed for cribra orbitalia, porotic hyperostosis, and enamel hypoplasias. Samples were collected for ongoing aDNA, stable isotope, and calculus research.

References for Supporting Information

1. Wentworth CK (1922) A scale of grade and class terms for clastic sediments. *The Journal of Geology* 30:377-392.
2. Munsell Soil Color Charts (2000) Revised Washable Edition. Munsell Color Company, Gretag Macbeth, New Windsor, New York: 35 pp.
3. Nelson C (1995) The work of the Koobi Fora Field School at the Jarigole pillar site. *Kenya Past and Present* 27:49-63.
4. Conyers LB (2013) *Ground-penetrating Radar for Archaeology, Third Edition*. Rowman and Littlefield Publishers, Alta Mira Press, Latham, Maryland.
5. Bird MI, Ayliffe LK, Fifield K, Cresswell R, Turney C (2003) Radiocarbon dating of organic- and carbonate-carbon in *Genyornis* and *Dromaius* eggshell using stepped combustion and stepped acidification. *Quaternary Science Reviews* 22:1805–1812.
6. Janz L, Elston RG, Burr GS (2009) Dating Northeast Asian surface assemblages with ostrich eggshell: implications for palaeoecology and extirpation. *Journal of Archaeological Science* 36:1982–1989.
7. Wang H, Hackley KC, Panno SV, Coleman DD, Liu JC-L, Brown J (2003) Pyrolysis combustion ^{14}C dating of soil organic matter. *Quaternary Research* 60:348–355.
8. Richards PDG, Richards PA, Lee ME (2000) Ultrastructural characteristics of ostrich eggshell: Outer shell membrane and the calcified layers. *Journal of the South African Veterinary Association* 71:97–102.
9. Jain S, Bajpai S, Kumar G, Pruthi V (2016) Microstructure, crystallography and diagenetic alteration in fossil ostrich eggshells from Upper Palaeolithic sites of Indian peninsular region. *Micron* 84:72–78.
10. Southon JR (2007) Graphite reactor memory – where is it from and how to minimize it? *Nuclear Instruments and Methods in Physics Research B* 259:288–292.
11. Stuiver M, Polach H (1977). Reporting of ^{14}C data. *Radiocarbon* 19:355–363.
12. Bronk Ramsey C (2009) Bayesian analysis of radiocarbon dates. *Radiocarbon* 51:337–360.
13. Reimer PJ et al. (2013) IntCal13 and Marine13 radiocarbon age calibration curves 0–50,000 years cal BP. *Radiocarbon* 55:1869–1887.
14. Williamson RF, Pfeiffer S (2003) Bones of the ancestors: The archaeology and osteobiography of the Moatfield ossuary. *Archaeological Survey of Canada. Mercury Series Paper*, *163*.
15. Buikstra JE, Ubelaker DH (1994) *Standards for Data Collection from Human Skeletal Remains.* Arkansas Archaeological Survey Research Series, Fayetteville.
16. White TD, Black MT, Folkens PA (2012) *Human Osteology*, 3rd ed. Academic Press, Amsterdam.
17. AlQahtani SJ, Hector MP, Liversidge HM (2010) Brief communication: the London atlas of human tooth development and eruption. *American Journal of Physical Anthropology* 142:481–490.
18. Scheuer L, Black S (2000) *Juvenile Osteology*. Academic Press, San Diego.